IEEE Access
The journal for rapid open access publishing

Received July 9, 2014, accepted August 1, 2014, date of publication August 27, 2014, date of current version September 9, 2014.

Digital Object Identifier 10.1109/ACCESS.2014.2352614

Microwave System for the Early Stage Detection of Congestive Heart Failure

SASAN AHDI REZAEIEH, (Student Member, IEEE), KONSTANTY S. BIALKOWSKI, (Member, IEEE), AND AMIN M. ABBOSH, (Senior Member, IEEE)

School of Information Technology and Electrical Engineering, University of Queensland, Brisbane, QLD 4072, Australia

Corresponding author: S. A. Rezaeieh (s.ahdirezaeieh@uq.edu.au).

ABSTRACT Fluid accumulation inside the lungs, known as cardiac pulmonary edema, is one of the main early symptoms of congestive heart failure (CHF). That accumulation causes significant changes in the electrical properties of the lung tissues, which in turn can be detected using microwave techniques. To that end, the design and implementation of an automated ultrahigh-frequency microwave-based system for CHF detection and monitoring is presented. The hardware of the system consists of a wideband folded antenna attached to a fully automated vertical scanning platform, compact microwave transceiver, and laptop. The system includes software in the form of operational control, signal processing, and visualizing algorithms. To detect CHF, the system is designed to vertically scan the rear side of the human torso in a monostatic radar approach. The collected data from the scanning is then visualized in the time domain using the inverse Fourier transform. These images show the intensity of the reflected signals from different parts of the torso. Using a differential based detection technique, a threshold is defined to differentiate between healthy and unhealthy cases. This paper includes details of developing the automated platform, designing the antenna with the required properties imposed by the system, developing a signal processing algorithm, and introducing differential detection technique besides investigating miscellaneous probable CHF cases.

INDEX TERMS Congestive heart failure, microwave imaging, UHF antenna, pulmonary edema.

I. INTRODUCTION

Microwave techniques for imaging and detection have the potential to be promising diagnostic tools for many medical applications. Besides being low cost, low profile and portable, their non-ionizing radiation characteristics enable long term monitoring, imaging and detection of various diseases such as breast cancer, brain stroke, and congestive heart failure (CHF) [1]–[10].

CHF is one of the main causes of death [11], and yet there is a lack of a comprehensive study on the application of microwave techniques on the detection of early stage CHF. One of the main symptoms of CHF is the accumulation of fluids (Cardiac Pulmonary Edema) inside the air sacs in the lungs as depicted in Fig. 1. When the heart fails to supply enough blood, pressure increases in the blood vessels near the lungs. This results in a gradual leakage of blood into air sacs of the lungs. Accumulation of blood increases the pressure in the capillaries, which are the tiniest blood vessels in the body and consequently causes leakage of fluid (mainly water) inside the lungs, known as cardiac pulmonary edema. This phenomenon changes the effective electrical properties of the affected lungs significantly due to the large contrast between the electrical properties of the accumulated fluids compared with the lung's tissues.

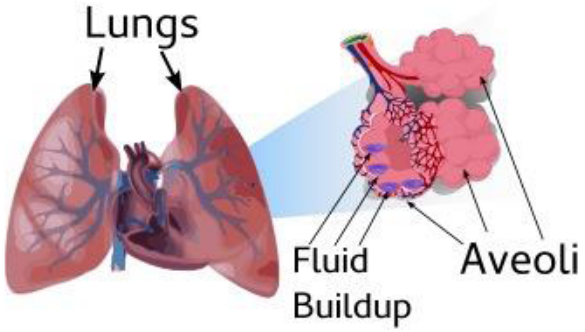

FIGURE 1. Fluid accumulation inside lungs in early stage heart failure.

Various studies have been conducted on detecting the fluid accumulation in the lungs as an early sign of CHF. The simplest way suggested in the literature involves mapping the changes in the amplitude of the reflected or transmitted signal

from or through the human torso, respectively [10], [12]. However, that technique is sensitive to the positioning of the measuring setup and surrounding medium and hence is not reliable. Another technique which has been investigated for a quite long time involves monitoring changes in the phase of the reflected or transmitted signal from or through the torso. However, that approach, shows only very small changes in phase that need to be detected over a long period of monitoring; an approach that is not reliable as that small phase change can be overweighed by any small change in the measuring setup, the human body, or the surrounding environment. Moreover, that limited phase difference was obtained in experiments using an oversimplified torso and applying the microwave sensor directly on the lungs, without considering the effects of muscles, ribs and skin layer. In another approach, acoustic techniques have been investigated [13]. However, there has been limited success in building a fully operational system that can be tested on a realistic torso to verify the reliability of the technique [14].

This paper presents the design of an automated and operational system, which provides a novel solution to detect and locate the presence of fluid inside the lungs as an early symptom of CHF. The applied method utilizes the frequency dependent scattering profile obtained by sending and capturing a wideband signal into the torso over a scan area. The basis of the used techniques is the fact that lungs' tissues and accumulated fluid have a large difference in their electrical properties; these changes can be revealed in the scattering profile of a monostatic-radar approach. However, the scattering profiles themselves are small compared to the total reflection caused by other parts of the body. So, to visualize them clearly, a differential technique that compares the scattering profile of the left and right side lungs is used. Based on a parameter study of healthy and varying levels of unhealthy cases, a threshold is proposed to differentiate between healthy and unhealthy cases. Using this threshold, the lowest detectable amount of fluid is determined (system limitation). All probable cases of CHF are investigated using realistic torso phantom and corresponding imaging results are reported. The proposed system operates in the ultra-high frequency (UHF) band of 0.77 – 1 GHz, which offers a reasonable compromise between the required penetration of low power microwave signals and acceptable resolution of the acquired images [15].

II. ELEMENTS OF THE HEART FAILURE DETECTION SYSTEM

A block diagram of the system is shown in Fig. 2. The system is controlled by a laptop PC which is connected to a portable and custom made microwave transceiver via a USB cable on one side, and to a stepper motor via an Ethernet cable on the other side. Using a coaxial cable, the microwave transceiver is connected to an antenna that is attached to the automated vertical scanning platform in the form of a linear rail that is moved by the afore-stated stepper motor. The antenna, which is designed specifically for the system, operates between

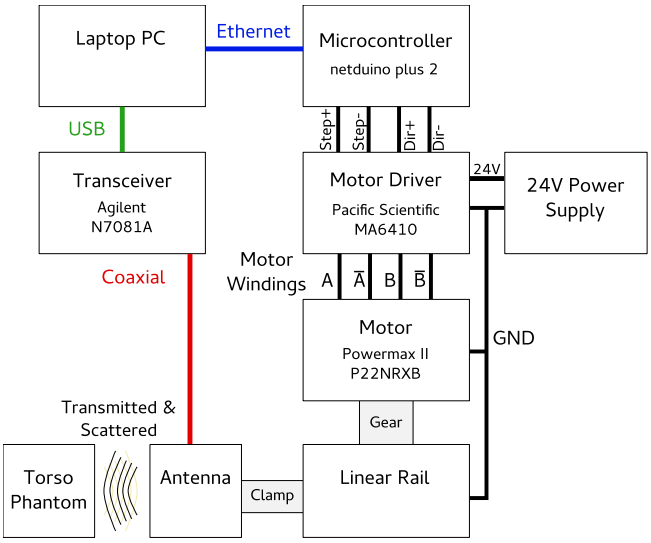

FIGURE 2. Block diagram of the system.

0.77 GHz and 1 GHz and is located at a certain distance "d" from the torso phantom.

The designed system operates in a way that the transceiver with the antenna operates as monostatic radar. It sends microwave signals towards, and receives the backscattered signals from, the torso. The frequency dependent backscattered signals are converted to time domain signals and then visualized as radargram images. These images show the intensity of scattering within different regions in the torso and can be used to assess the health condition of the torso.

A. ANTENNA

The antenna as an important element of this system is expected, if designed using the conventional methods, to have a large size as it operates at the lower UHF band. Moreover, considering the limited allowed microwave power in medical applications for safety reasons, the antenna is required to radiate the power efficiently in the forward direction. Thus, it needs to have a unidirectional radiation. Moreover, it should possess a wide operating bandwidth to provide an acceptable resolution for the obtained images.

An extensive literature review reveals several research articles on unidirectional antennas operating at UHF band [16]–[21]. Various techniques were implemented in order to obtain a unidirectional radiation pattern while not affecting the operating bandwidth of the antenna. The most dominant technique is locating a reflector a quarter wavelength distance from the antenna [16]. However, using such a reflector for antennas operating at the lower UHF frequencies increases their size drastically. Instead, a folding technique is applied in this paper to realize a compact antenna as explained hereafter.

Considering the lower end of the utilized frequency band, the initial antenna structure [22] in the form of planar slotted patch was designed on a RO4003 substrate with a dielectric

constant of 3.55, a thickness of 0.8 mm and a loss tangent of 0.0027 and dimensions of 140 × 140 × 0.8 mm^3.

Using the simulator HFSS, a CPW feed-line with a length of ℓ_f, which was separated from the ground conductor by a gap of g = 0.25 mm for a 50 Ω input impedance was extended into the substrate at the top layer (above the ground plane) by a length of ℓ_g (see Fig. 3) in order to achieve a good input impedance match. Employing an asymmetric monopole CPW-fed antenna design, the main radiator of the antenna with a length of approximately λ/4 = 94 mm was connected to the feedline (where λ is the free space wavelength of the first resonance of the antenna). This design was designated as Antenna 1, as shown in Fig. 4.

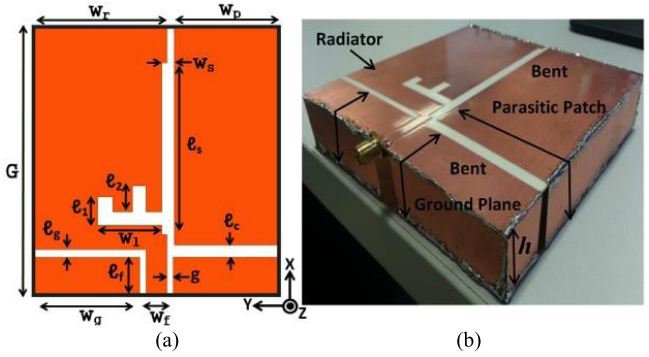

FIGURE 3. (a) Top view and (b) 3-D prototype of the proposed antenna.

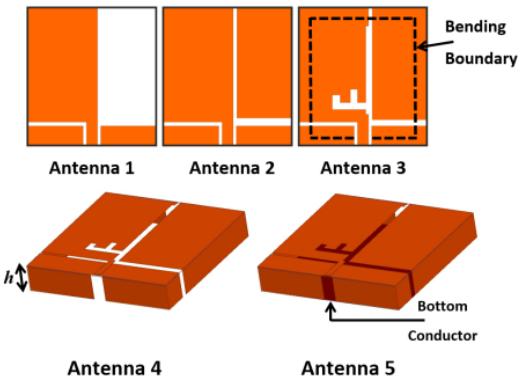

FIGURE 4. Evolution process of Antenna 1 to Antenna 5.

To explain the performance of the antenna in terms of its resonance frequencies, the imaginary and real parts of the input impedance are presented in Fig. 5. Antenna 1 has a matched resonance ($\mathrm{Im}\{Z_{in}\} = 0\,\Omega, \mathrm{Re}\{Z_{in}\} \approx 50\,\Omega$) around 700 MHz and a mismatched resonance ($\mathrm{Im}\{Z_{in}\} = 0\ \Omega$, $\mathrm{Re}\{Z_{in}\} \neq 50\ \Omega$) around 1100 MHz. Therefore, to excite and reveal the second resonance, and consequently increase the operating bandwidth of the antenna, a metallic patch was added adjacent to the main radiator, as shown for the antenna designated as Antenna 2 in Fig. 4. The parasitic patch was used to excite the second mode of the main radiator. To further increase the operating bandwidth, given the current distribution on the radiator and in order to increase the main current path, an F-shaped slot and a straight longitudinal slot were created on the radiating patch. This configuration was designated as Antenna 3. As illustrated in Fig. 6, adding the aforementioned slots makes the main current path longer on Antenna 3 compared to the one on Antenna 2. Consequently, the former configuration achieves a second 50 Ω input impedance match at about 950 MHz, as shown in Fig. 5.

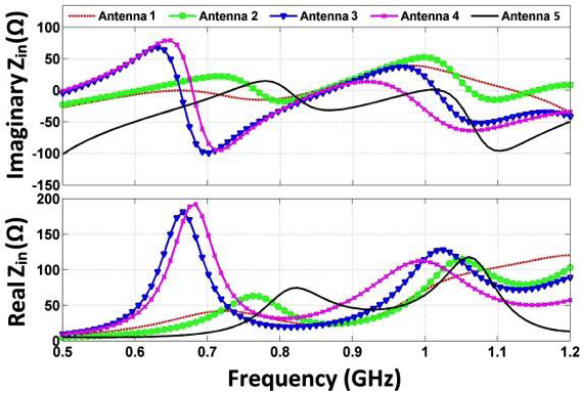

FIGURE 5. Real and imaginary parts of the input impedance of Antennas 1 to 5.

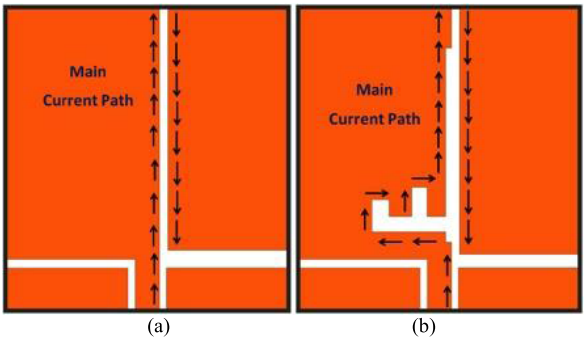

FIGURE 6. Main current paths of (a) Antenna 2, and (b) Antenna 3.

To comply with the principal requirements of the current design, Antenna 3 had to be modified to occupy less physical space and to suppress the back radiation, resulting in unidirectional patterns. To fulfill the compact size requirement without affecting the impedance matching and the radiation efficiency, Antenna 3 was bent along its four edges, as indicated by the black bending boundary in Fig. 4, resulting in Antenna 4. It was found that a height of h = 20 mm, did not affect the main radiation characteristics and impedance matching performance of the antenna to a great extent. Bending the antenna reduced its overall size by 33% to 120 × 120 × 20 mm.

To fulfill the unidirectional radiation pattern requirement, a common technique was employed, where a conducting plane was located on the bottom side of the antenna at a height of h, and this was designated as Antenna 5, as shown in Fig. 4. As depicted in Fig. 7, the height h had a great effect

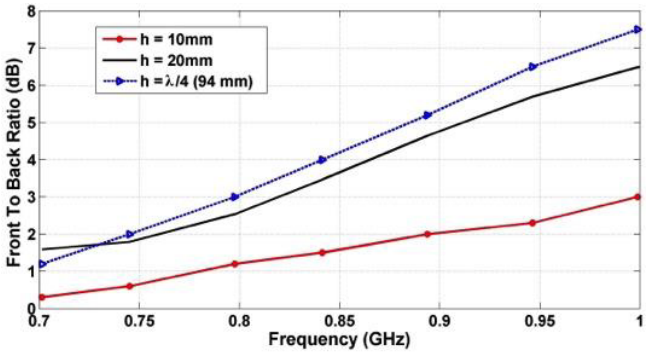

FIGURE 7. Simulated front-to-back ratio of Antenna 5 for different values of *h*.

on the radiation characteristics of the antenna. Compromising between the size, impedance matching and the directivity of the antenna, initial investigations of the height h revealed that unidirectional radiation characteristics could be obtained for a height of $h = 20$ mm, which were nearly the same as for the $h = \lambda/4$ (94 mm) case. Based on the aforementioned discussion and the design requirements, the optimum dimensions of the final design (Antenna 5) are presented in Table 1.

TABLE 1. Final dimensions for antenna 5 shown in Fig. 1 (Units: mm).

ℓ_1	10	ℓ_g	3	W_p	55
ℓ_2	10	W_f	5	W_s	5
ℓ_c	5	W_g	57.25	G	120
ℓ_f	23	W_r	62.5	h	20
ℓ_s	90	W_1	30	g	0.25

As depicted in Fig. 8, the antenna has a measured impedance bandwidth with $|S_{11}| < -10$ dB over the range of 0.77 GHz to around 1 GHz and depicts a measured gain (+z direction) between 2.6 and 5 dBi and the measured efficiency is more than 70 %.

B. PLATFORM

The system measurement is controlled by a laptop with MATLAB installed. It controls both the data acquisition device as well as the automatic antenna positioning. Data acquisition is performed using an Agilent N7081A microwave transceiver connected via USB. This device has a functionality that is similar to the conventional, but costly, vector network analyser. Moreover, it is compact and can be easily connected to a laptop for automated testing of a portable system. The frequency range of the transceiver is from 0.1 to 4 GHz with around 80 dB of dynamic range. In our system, the device is used to gather the frequency dependant scattering parameters over the operating frequency band of the antenna, which is from 0.77 GHz to 1 GHz.

The automatic antenna positioning is performed using a linear rail which is driven using a stepper motor. The stepper motor is a Powermax II P22NRXB, which has a step size of 1.8 degrees and a maximum speed of 1500 RPM. The stepper

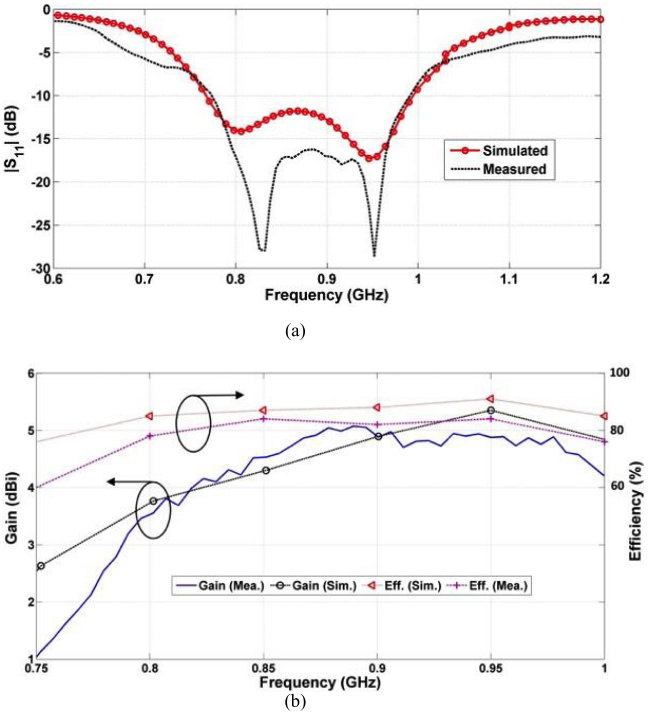

FIGURE 8. (a) Reflection coefficient and (b) gain and efficiency of Antenna 5.

motor is an eight-pin motor and is connected using series windings. A Pacific Scientific 6410 Step Drive controls this motor using a 2.5 Amp output mode [23]. The step drive converts step and direction inputs from an embedded processor to the required motor winding currents for the stepper motor. The embedded processor providing these inputs is a netduino plus 2, which features an ARM Cortex M4 based platform running at 168 MHz and has 100 kB of RAM and 384 kB of flash storage [24]. This embedded processor is connected to the laptop via an Ethernet based network connection, and is controlled using transmission control protocol (TCP) network packets.

The positioning of the antenna on the linear rail was found to require 85 motor steps per millimetre, meaning that for each measurements the motor is stepped 850 times to achieve 10 mm motion between measurements.

C. DATA ACQUISITION

The data acquisition process is performed using a single script inside MATLAB which is depicted as flowchart in Fig. 9. The process begins with calibrating the microwave transceiver using a standard 1-port calibration procedure of open, short and load at the end of the coaxial cable which feeds the antenna. This calibration process is done to eliminate the undesired signals such as internal reflections of the antenna and antenna-air signal distortions.

Next, the data acquisition process is performed which involves the acquisition of 21 measurements in the vertical (y) direction, each separated by 10 mm and totaling to a scan

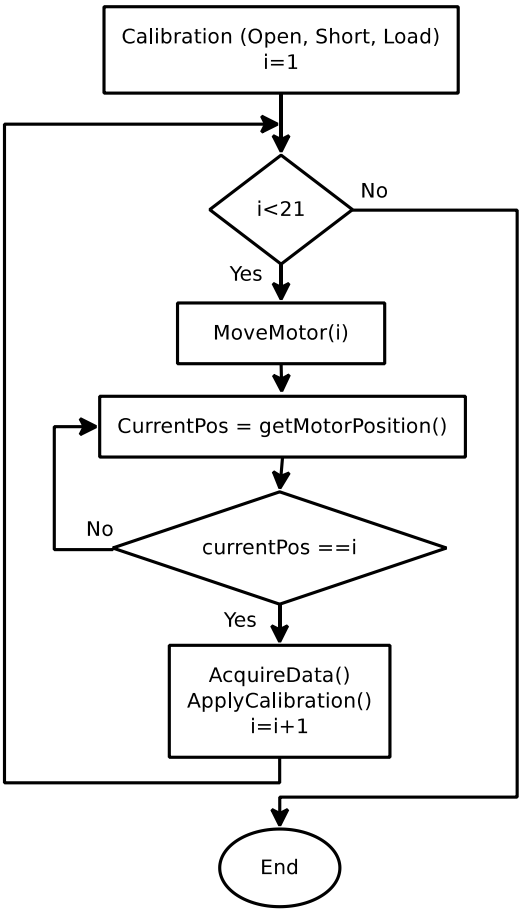

FIGURE 9. Flowchart of data acquisition procedure.

distance of 210 mm. For each measurement, the data is first acquired by the microwave transceiver, and then a command is sent to embedded system to move the linear rail 10 mm. To synchronize the position with measurements, status packets are requested by the laptop to ensure that the motor has finished moving before the measurement is taken and subsequent motion commands.

III. TORSO PHANTOM

To test the designed system in the lab, a torso phantom is required. In the present literature, single layered homogenous phantoms such as the one from SPEAG, Switzerland, have been used. However, in this paper, we used a realistic torso phantom for testing the system. As depicted in Fig. 10, the utilized phantom is an anatomical model with analogues size to that of a human torso with 43 $\times$ 40 $\times$ 48 cm^3 dimensions with a chest circumference of 94 cm. It includes the main cardiovascular organs such as fat, ribs, abdomen, lungs and heart. The soft tissues and bones are fabricated using polyurethane and epoxy resin, respectively. The phantom is originally designed by the company Kyoto Kagako, Japan for testing CT scan systems [21], [25].

In our work, the phantom is used for electromagnetic (EM) based imaging, which requires an accurate emulation of the electrical properties of the human torso across the utilized

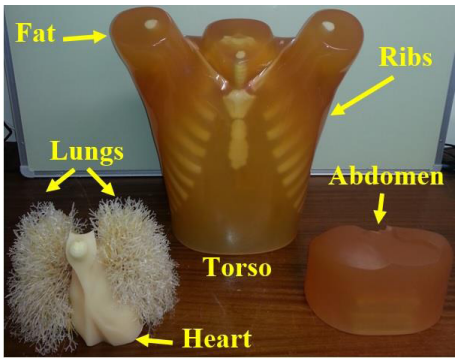

FIGURE 10. Torso phantom.

frequency band. The suitability of this phantom was confirmed by testing the electrical properties (permittivity and conductivity) of its parts using Agilent 85070E dielectric probe kit. We found that the phantom provides, not a perfect but reasonable dispersive properties. More importantly, the phantom represents a complex environment analogous to a real torso thus providing an excellent test environment for the designed system.

IV. DATA PROCESSING AND ANALYSIS

In the proposed system, the acquired data (backscattered signals) is recorded as frequency dependent scattering parameters. The first step of processing involves the conversion of each measurement to time domain using an inverse Fourier transform. It should be noted that as the scattering parameters are normalized unit-less quantities, the inverse Fourier transform is also normalized unit-less quantities that correspond to the correlation between the transmitted and scattered pulses. In the experimental results presented in this paper, the inverse Fourier transform has been scaled to propagation distance in millimeters. Each of these time domain measurements overlaid on top of each other is shown in the top part of Fig. 11. By combining the time domain measurements, or traces, over a scan distance, the resulting image is a radargram. Such an

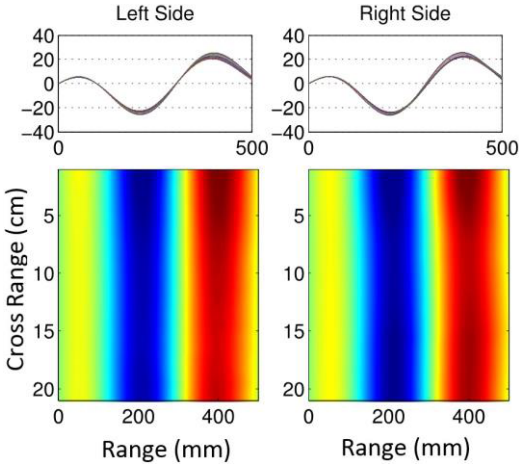

FIGURE 11. A typical radargram.

image, as depicted in the lower part of Fig. 11, shows the scattered wave power delay profile along a set of recorded positions.

A precise linear scan is performed by using the stepper motor and linear rail. Hence any error in the measurement is dependent only on the noise and the accuracy of phantom positioning relative to the antenna.

To visualize the healthiness of the lungs, the difference between the left and right scan or a difference in the radargrams between the left and right side of the torso, is used. This differential process provides a clearer picture, as the changes, that may exist, are small variations in phase and amplitude compared to the total scattered signal due to the small size of the target (fluid) to be detected in early stage CHF. The resulting difference can be thought of as a likelihood of whether the left or right side has larger reflections or scattering, at different locations in the lung. Where a high positive value (shown in red) is obtained, it depicts a strong scattering on the left side of the lung at that location, whereas a large negative value (shown in blue) indicates the stronger scattering is present on the right side at that location. However, to keep consistency of results, high positive value (red) is used as a sign of presence of water in all cases.

In a healthy case, the tissue distributions of the left and right sides are close, and provide a comparable scattering profile. However, small differences are present due to the heart being present on the left side of the body (see Fig. 10). Without using sophisticated signal processing, detectable changes in water accumulation need to provide a scattering difference above this level. Consequently, the monitoring and detection time becomes almost instant. It takes less than three minutes to scan single lung, and less than five seconds to obtain the radargrams using a laptop with ordinary processing capability.

To make sure of the safe use of the proposed system when tested on human subjects, the specific absorption rate (SAR) is calculated using the available human body model in HFSS. This numerical model comprises of over 300 parts covering the whole cardiovascular organs under investigation. To that end, the designed antenna is placed in the vicinity of the torso model in the simulation environment in an analogous distance to that of the experimental setup. Following the usual procedure [1], the SAR values are calculated when using the selected frequency band with a transmitted power of 1mW. The maximum attained SAR value is found 0.06 W/Kg which is well below the safe threshold defined by IEEE [26].

V. EXPERIMENTS AND RESULTS

The complete experimental setup and integrated devices are depicted in Fig. 12.

A. SYSTEM CALIBRATION

As mentioned before, prior to data acquisition, the system is calibrated in the used frequency range of 0.77 – 1 GHz. To start the experiment, the torso phantom is located at a distance d = 10 mm from the antenna. This distance is

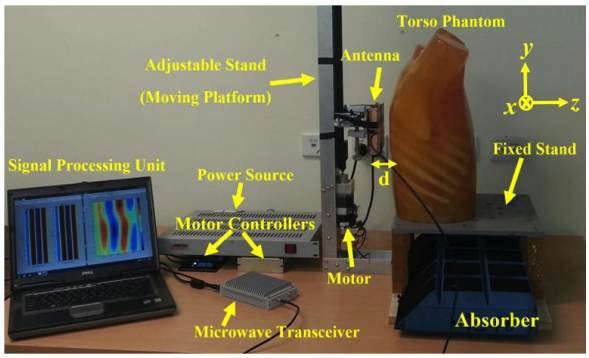

FIGURE 12. The designed congestive heart failure detection system.

optimized during the experiment process to obtain the best imaging results. To eliminate any source of error in the detection process, several similar experiments were conducted on the phantom to ensure that the same experiment can be repeated with minimal errors. To that end, the phantom was scanned by the antenna using the automated stand. The same scan was repeated several times. The difference between two consecutive scans is depicted in Fig. 13(a). The maximum error is less than 0.25. This maximum error value will be added to the threshold to obtain rigorous detection decisions. This error value can vary with both the antenna gain and distance separating the phantom structure and the antenna. This value is also related to the ratio of transmitted to scattered power and henceforth, is not dependent on the transmitted power. Therefore, the error value is neither a fixed nor standardized value, and is thus specific for the current system. Therefore, it needs to be calibrated and redefined when any system element, e.g. antenna, is replaced. The same would apply to all of the values of the radargrams presented in this section.

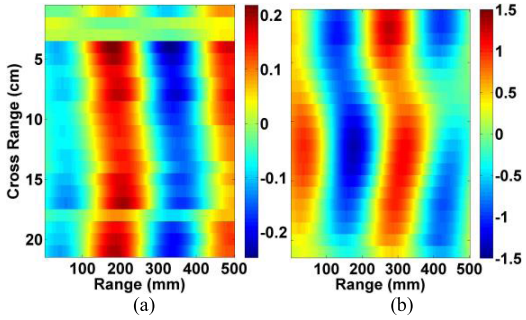

FIGURE 13. Differential scattering profile of (a) measurement error and (b) healthy case.

Using the differential method, the difference between the scattering profile of left and right side lungs of a healthy case were obtained. In this case, there is no water inserted inside the phantom. As depicted in Fig. 13(b), and as predicted, due to the partial presence of heart inside the left lung, a difference of maximum of 1.5 is observed. This value is verified through several experiments. Therefore, a detection threshold of 1.75 (healthy + error) is designated for the current system.

B. MINIMUM DETECTABLE LEVEL OF FLUID ACCUMULATION

To determine the minimum detectable level of fluid accumulation in the lungs and to verify whether the designed system is able to detect early stage CHF, many experiments using different amounts of fluids inserted inside one, or both of the lungs in plastic bags, were performed.

In those experiments, successively smaller amounts of water are located in the top portion of the left lung (arbitrary position) starting with 10 mL. In Fig. 14(a), the difference in the scattering profile for a case of 10 mL has strength of +6. This scattering profile is four times stronger than that of the healthy case (1.5). Rescaling the scattering profile of a healthy case (see Fig. 14(b)) to that of an unhealthy case shows detection of water on the top portion of the torso.

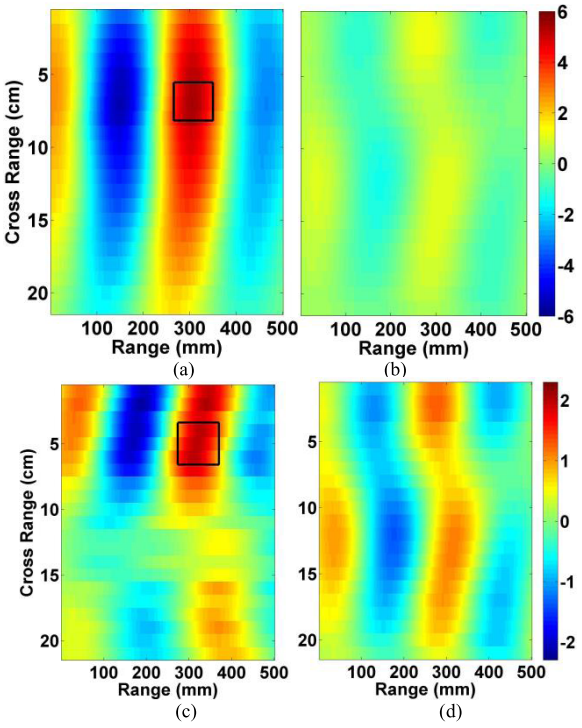

FIGURE 14. Differential scattering profile of lowest detectable fluid compared to healthy cases with identical scaling, (a) 10 mL water, (b) healthy and (c) 4 mL water, (d) healthy.

To push the limits of the system, the amount of the emulated water was further reduced. Through extensive experiments, it was found that 4 mL is the smallest detectable amount. As depicted in Fig. 14(c), the strength of the scattered signal from inner tissues of the torso is 2.5, which is 0.6 times stronger than the healthy case. Comparing the differential scattering profile of healthy (Fig. 14(d)) and unhealthy (Fig. 14(c)), a larger change is present at the top portion of the lung, where water was located (arbitrary position). The location of the water is depicted by a black rectangle in this and all upcoming figures. By reducing the amount of water to less than 4 mL, the strength of the reflected signals falls to under the threshold region which is counted as undetectable case. The scattering profile of this case is not depicted due to its similarity to the one of the healthy case.

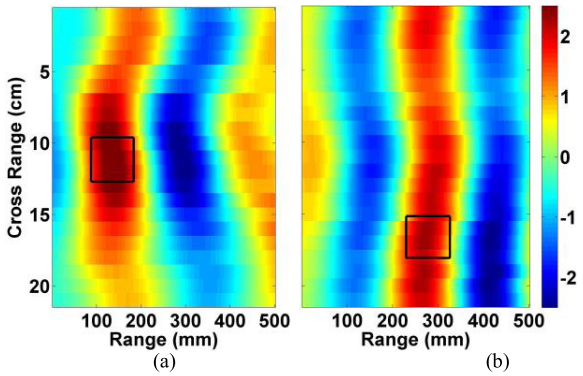

FIGURE 15. Detecting presence and position of water in two cases, (a) water located at middle rear side of phantom and (b) water located at lower front side of the phantom.

C. FLUID LOCALIZATION

To examine the capability of the system in positioning the accumulated fluid in addition to its detection, another experiment was conducted. A plastic bag containing the smallest detectable water amount (4 mL) was located in the middle of the rear side of the torso phantom. In the second case, the plastic bag is located in the lower front side of the phantom. The differential scattering profiles of investigated cases are depicted in Fig. 15. It can be seen that the strength of the signal is analogous to the previously detected 4 mL water content. However, the location of the water varies, which verifies the positioning ability of the system.

D. DETECTION IN THE CASE OF PRESENCE OF FLUID IN BOTH LUNGS

One of the cases which may occur, is the occasion where, there is fluid accumulation in both lungs. Considering the fact that due to gravity dependency and lung geometries, the possibility of fluid accumulation in both lungs with exactly the same value is near zero, the current system can be efficient

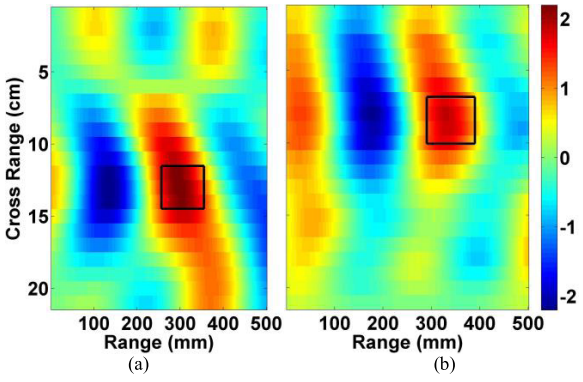

FIGURE 16. Detecting presence and position of fluid in cases of accumulation inside both lungs, (a) water content with 7 mL difference (b) water content with 4 mL difference.

in detecting the presence of water using similar differential method. In that regard, two plastic bags with two different water contents, 15 and 8 mL, were located in the left and right lungs, respectively. From Fig. 16(a), it can be seen that the scattering profile has a strength of 3.5 which is more than two times stronger than a healthy case. To push the limits of the system, the water content difference was reduced to 4 mL. From Fig. 16(b), one could easily locate the water in the middle of the lungs. The same limit (4 mL) applies for the detection of water in the case of presence of fluid in both lungs.

VI. CONCLUSION

The design, implementation and verification of an automated ultra-high frequency (UHF) microwave-based early stage congestive heart failure (CHF) monitoring and detecting system has been presented. The hardware of the system comprises a controllable scanning stand, a specifically designed unidirectional antenna, a portable custom-made microwave transceiver and a laptop. The software part of the system includes control, signal processing and visualizing algorithms. In this system, the antenna scans vertically the rear side of a human torso resembling phantom and gathers the backscattered signals from it. These signals are then translated into images showing the scattering profile inside the torso. This system operates based on the fact that fluid accumulated at the onset of CHF has higher dielectric constant compared to its surrounding tissues inside the torso, and consequently its scattering profile is stronger. Considering the fact that backscattered signals are quite weak, a differential approach is proposed to magnify the results. In this method, the differences between the scattering signal profiles received from left and right side lungs are obtained by subtracting them from each other. Based on these differences, a threshold is defined to make decisions on healthy and unhealthy cases. It has been shown that that the current system can detect as low as 4 mL of water inside the lungs; this value represents the early stage CHF. The possibility of accumulation of fluid on both lungs has also been studied. Considering its detection strength, low cost, portability and fast detection time, the current system has the potential to be an effective diagnostic tool especially in emergency units, GP clinics and rural areas.

ACKNOWLEDGMENT

The authors acknowledge the company Agilent Technologies, USA for providing the custom-made microwave sensor (N7081A) used in the experiments.

REFERENCES

[1] B. J. Mohammed, A. M. Abbosh, S. Mustafa, and D. Ireland, "Microwave system for head imaging," *IEEE Trans. Instrum. Meas.*, vol. 63, no. 1, pp. 117–123, Jan. 2014.

[2] S. Mustafa, B. Mohammed, and A. Abbosh, "Novel preprocessing techniques for accurate microwave imaging of human brain," *IEEE Antennas Wireless Propag. Lett.*, vol. 12, pp. 460–463, Mar. 2013.

[3] S. Mustafa, A. M. Abbosh, and P. T. Nguyen, "Modeling human head tissues using fourth-order Debye model in convolution-based three-dimensional finite-difference time-domain," *IEEE Trans. Antennas Propag.*, vol. 62, no. 3, pp. 1354–1361, Mar. 2014.

[4] S. Salman, Z. Wang, E. Colebeck, A. Kiourti, E. Topsakal, and J. L. Volakis, "Pulmonary edema monitoring sensor with integrated body-area network for remote medical sensing," *IEEE Trans. Antennas Propag.*, vol. 62, no. 5, pp. 2787–2794, May 2014.

[5] N. Celik, R. Gagarin, G. C. Huang, M. F. Iskander, and B. W. Berg, "Microwave stethoscope: Development and benchmarking of a vital signs sensor using computer-controlled phantoms and human studies," *IEEE Trans. Biomed. Eng.*, vol. 61, no. 8, pp. 2341–2349, Aug. 2014.

[6] M. F. Iskander, R. Maini, C. H. Durney, and D. G. Bragg, "A microwave method for measuring changes in lung water content: Numerical simulation," *IEEE Trans. Biomed. Eng.*, vol. 28, no. 12, pp. 797–804, Dec. 1981.

[7] A. H. Golnabi, P. M. Meaney, and K. D. Paulsen, "Tomographic microwave imaging with incorporated prior spatial information," *IEEE Trans. Microw. Theory Techn.*, vol. 61, no. 5, pp. 2129–2136, May 2013.

[8] D. Ireland and A. Abbosh, "Modeling human head at microwave frequencies using optimized Debye models and FDTD method," *IEEE Trans. Antennas Propag.*, vol. 61, no. 4, pp. 2352–2355, Apr. 2013.

[9] Y. Wang, A. M. Abbosh, B. Henin, and P. T. Nguyen, "Synthetic bandwidth radar for ultra-wideband microwave imaging systems," *IEEE Trans. Antennas Propag.*, vol. 62, no. 2, pp. 698–705, Feb. 2014.

[10] C. Susskind, "Possible use of microwaves in the management of lung disease," *IEEE Proc.*, vol. 61, no. 5, pp. 673–674, May 1973.

[11] V. L. Roger *et al.*, "Trends in heart failure incidence and survival in a community-based population," *J. Amer. Med. Assoc.*, vol. 292, no. 3, pp. 344–350, Jul. 2004.

[12] P. C. Pedersen, C. C. Johnson, C. H. Durney, and D. G. Bragg, "Microwave reflection and transmission measurements for pulmonary diagnosis and monitoring," *IEEE Trans. Biomed. Eng.*, vol. BME-25, no. 1, pp. 40–48, Jan. 1978.

[13] Y. Feng *et al.*, "Lung water detection using acoustic techniques," in *Proc. IEEE Annu. Int. Conf. Eng. Med. Biol. Soc. (EMBC)*, Aug./Sep. 2012, pp. 4258–4261.

[14] S. A. Rezaeieh, A. Abbosh, and Y. Wang, "Wideband unidirectional antenna of folded structure in microwave system for early detection of congestive heart failure," *IEEE Trans. Antennas Propag.*, doi: 10.1109/TAP.2014.2342756.

[15] S. A. Rezaeieh, Y. Q. Tan, A. Abbosh, and M. A. Antoniades, "Equivalent circuit model for finding the optimum frequency range for the detection of heart failure using microwave systems," in *Proc. IEEE Proc. APS-URSI*, Orlando, FL, USA, Jul. 2013, pp. 2059–2060.

[16] S.-W. Qu, J.-L. Li, Q. Xue, C. H. Chan, and S. Li, "Wideband and unidirectional cavity-backed folded triangular bowtie antenna," *IEEE Trans. Antennas Propag.*, vol. 57, no. 4, pp. 1259–1263, Apr. 2009.

[17] G.-M. Zhang, J.-S. Hong, B.-Z. Wang, G. Song, and P. Zhang, "Compact wideband unidirectional antenna with a reflector connected to the ground using a stub," *IEEE Antennas Wireless Propag. Lett.*, vol. 10, pp. 1186–1189, Oct. 2011.

[18] S. A. Rezaeieh and A. M. Abbosh, "Wideband and unidirectional folded antenna for heart failure detection system," *IEEE Antennas Wireless Propag. Lett.*, vol. 13, pp. 844–847, Apr. 2014.

[19] J. Wu, Z. Zhao, Z. Nie, and Q. H. Liu, "A broadband unidirectional antenna based on closely spaced loading method," *IEEE Trans. Antennas Propag.*, vol. 61, no. 1, pp. 109–116, Jan. 2013.

[20] N. Celik, R. Gagarin, Y. Hyoung-sun, and M. F. Iskander, "A noninvasive microwave sensor and signal processing technique for continuous monitoring of vital signs," *IEEE Antennas Wireless Propag. Lett.*, vol. 10, pp. 286–289, Mar. 2011.

[21] S. A. Rezaeieh, K. S. Bialkowski, and A. M. Abbosh, "Folding method for bandwidth and directivity enhancement of meandered loop ultra-high frequency antenna for heart failure detection system," *IET Microw. Antennas Propag.*, Jul. 2014, doi: 10.1049/iet-map.2014.0340

[22] S. A. Rezaeieh, A. Abbosh, and M. A. Antoniades, "Broadband UHF antenna for heart failure detection system," in *Proc. IEEE APS-URSI*, Jul. 2013, pp. 2089–2090.

[23] *MA6410 Installation & Hardware Reference Manual*, Pacific Scientific, Seattle, WA, USA, 1998

[24] *Secret Labs LLC 'Netduino Plus 2 Technical Specifications'*. [Online]. Available: http://netduino.com/netduinoplus2/specs.htm, accessed Apr. 22, 2014.

[25] K. Kagaku. *Multipurpose Chest Phantom: Lungman*. [Online]. Available: http://www.kyotokagaku.com/products/detail03/pdf/ph-1_catalog.pdf, accessed Apr. 17, 2014.

[26] *IEEE Committee on Radiation; Technical Information Statement on Human Exposure to Microwaves and Other Radio Frequency EM Fields*. [Online]. Available: http://ewh.ieee.org/soc/embs/comar/rf_mw.htm/, accessed Apr. 22, 2014.

SASAN AHDI REZAEIEH (S'11) received the M.S. degree in telecommunications engineering from Istanbul Technical University, Istanbul, Turkey, in 2012. He joined the Microwave Research Group at the University of Queensland, Brisbane, QLD, Australia in 2012, where he is currently pursuing the Ph.D. degree. His current research involves designing wideband antennas for microwave-based heart failure detection system. His research interests are antenna miniaturization for ultrahigh-frequency medical diagnostic applications.

KONSTANTY S. BIALKOWSKI received the dual B.Eng./B.Sc. (Hons.) degree and the Ph.D. degree in wireless communications from the University of Queensland, Brisbane, QLD, Australia, in 2003 and 2008, respectively. He was a Research Engineer with National ICT Australia, Melbourne, VIC, Australia, prior to joining the School of Information Technology and Electrical Engineering at the University of Queensland in 2009, where he is currently a Research Fellow. His research interests include near-field and passive radar systems, multiple element antenna systems, and wireless communications. He was a recipient of the Early CAREER Researcher Award at the 2011 Australian Communication Theory Workshop and the Highly Commended Presentation Award at the 2005 Australian Symposium on Antennas.

AMIN M. ABBOSH (SM'08) received the M.Sc. degree in communication systems and the Ph.D. degree in microwave engineering from Mosul University, Mosul, Iraq, in 1991 and 1996, respectively, and the Grad.Cert. degree in higher education and the Dr.Ing. degree from the University of Queensland, Brisbane, QLD, in 2008 and 2013, respectively. He is currently an Associate Professor, leader of the Microwave Group, and the Director of post-graduate studies with the School of Information Technology and Electrical Engineering, University of Queensland. He has authored over 250 papers on wideband passive microwave devices, planar antennas, and microwave-based imaging systems.